Journal of Materials Chemistry C

Transition of wide-band gap semiconductor h-BN(BN)/P heterostructure via single-atom-embedding

Journal:	*Journal of Materials Chemistry C*
Manuscript ID	TC-ART-05-2020-002371.R1
Article Type:	Paper
Date Submitted by the Author:	12-Jun-2020
Complete List of Authors:	Miyazato, Itsuki; Hokkaido Daigaku Kogakubu Daigakuin Kogakuin Kogaku Kenkyuin, Hussian, Tanveer; University of Western Australia, School of Chemistry and Biochemistry Takahashi, Keisuke; Hokkaido University, Department of Chemistry; National Institute for Materials Science, Center for Materials research by Information

Journal Name

ARTICLE TYPE

Cite this: DOI: 00.0000/xxxxxxxxxx

Transition of wide-band gap semiconductor h-BN(BN)/P heterostructure via single-atom-embedding†

Itsuki Miyazato,*[a] Tanveer Hussain,[b] and Keisuke Takahashi[a]

Received Date
Accepted Date

DOI: 00.0000/xxxxxxxxxx

The transition of band gap in boron nitride/phosphorene(h-BN/P) heterostructure are investigated by single-atom-embedding via first principles calculations. In particular, the single-atom-embedded heterostructures are designed by embedding 10 different single atoms between h-BN/P bilayers to compare the property transition against pure h-BN/P heterostructure. The thermodynamic evaluation reveals that embedding atom plays an important role for the stability in heterostructure formation. resulting that Na, Pd and Pt embedded heterostructures are energetically stable. The stable Na, Pd and Pt embedded h-BN(BN)/P heterostructures are subsequently evaluated in terms of their electronic structures for the comparison with pure h-BN(BN)/P heterostructure. The band gaps of the Na, Pd and Pt embedded heterostructures reveals to be lower (1.5∼1.8 eV) than wide-band gap pure h-BN/P heterostructure(=2.425 eV) with GLLB-sc functional calculation. The band gap engineering of h-BN/P heterostructure is novelly revealed through single atom doping, transform them into into promising photoelectric materials as solar energy conversion devices.

Introduction

The successful synthesis of graphene, an organic two dimensional materials expands the opportunities of designing inorganic materials[1]. While the graphene is the notable two dimensional materials[2], other two dimensional materials have been experimentally and computationally proposed such as germane[3,4], phosphorene[5–10], stanene[11–13] and Transition metal dichalcogenides(TMDCs)[14–17]. Those materials consist of unique physical and chemical properties leading to applications in electronic devices, such as semiconductors, optoelectronic devices, and sensors[18,19]. The design of two dimensional materials steps into the next level where heterostructured two dimensional materials have been designed by stacking the different two dimensional materials[20–22]. Materials such as Graphene/h-BN[23], h-BN(BN)/P, As/At[24], WSe_2/$MoSe_2$[25], stanene/CrI_3[26], and MoS_2/$CuInP_2S_6$[27], and BN/BX (X = P,As,Sb[28] are successful cases where unique physical and chemical properties are observed[8,27]. Moreover, different single-atom-embedded structures are proposed to tune the electronic properties of two dimensional heteorstructure[29,30]. Particularly, BN-P heterostructure has previously been sugessted as a potential photovoltaic application with first principle study by introducing alkali metal and alkali-earth metal[31]. However, no potential materials have been suggested when transition metal is introduced in h-BN/P heterostructure. Thus, in this study, several transition metals are introduced to explore the novel candidate materials. Here, single atom is embedded in bilayer h-BN/P two dimensional heterostructures is designed in term of tuning its electronic properties. In particular, Na, Pd, Pt, Sc, Sn, Ti, Ag, Al, Au, and Fe single atoms are embedded between h-BN and P layers in order to tune the electronic properties along the seeking the stable single atom between layers.

Computational method

All calculations are carried out within density functional theory(DFT) implemented in grid-based projector-augmented wave (GPAW) method[32]. All calculations are spin polarized and applied real space presentation(the finite difference mode). The periodic boundary condition is set under k-point of (4,4,1) Brillouin zone sampling[33] with grid spacing of 0.20 Å . The ground state structures are explored with the vdW-DF exchange correlation functional in order to consider the van der Waals interaction between layers[34]. The vacuum length is set 10 Å in z axis to avoid interaction between layers for all structure.

The bilayer heterostructured h-BN/P is designed by stacking orthogonal h-BN and phospherene single layer: The lattice is matched by repeating its cell in each other: 3 times in x-axis in primitive P layer, 4 times in x-axis and 2 times in y-axis in

[a] Department of Chemistry, Faculty of Science, Hokkaido University, Kita 10, Nishi 8, Kita-ku, Sapporo, 060-0810, Japan.; E-mail: miyazato@sci.hokudai.ac.jp
[b] School of Molecular Sciences, The University of Western Australia, Perth, WA, 6009, Australia.

† Electronic Supplementary Information (ESI) available: [details of any supplementary information available should be included here]. See DOI: 00.0000/00000000.

primitive h-BN layer. Note that applied two dimensional P structure is based on black phosphorus structure among the various characteristic 2D-P allotropes[35]. The lattice mismatch between h-BN(BN)/P layer is estimated by the following equation 1.

$$M_{lattice} = (1 - \frac{d_{2D-P}}{d_{BNP}}) \times 100 \quad (1)$$

where $M_{lattice}$, d_{2D-P}, and d_{BNP} represent lattice mismatch(%), lattice constant a(b) of single layer P, and lattice constant a(b) of bilayer h-BN(BN)/P heterostructure , respectively. Note that reference state of the system is BN layer : d_{BNP} is equal to the lattice constant a(b) of single layer h-BN. Finally, two layered h-BN/P heterostructure model (single layer h-BN and single layer phosphorene) is designed for the calculation. Single-atom-embedded models are designed by embedding Na, Pd, Pt, Sc, Sn, Ti, Ag, Al, Au, and Fe single atom between h-BN(BN)/P layers. Note that the embedded atoms are chosen in the reference of successful studies for material design by embedding single atom[30,36–40]. Two embedded sites are proposed to compare that how doped site interact its electronic structure. Thus, two models are finally designed for each single atom; Structure A:"doped atom embedded under B", and Structure B:"doped atom embedded under N"(See Figure 1). The embedded atom is placed on the bridge(dangling)-site of phosphorene layer due to its stability reported in previous studies on single layer phosphorene[9].Additionally, two types of sites are considered: a site under a B atom of the h-BN layer and a site under a N atom of the h-BN layer.

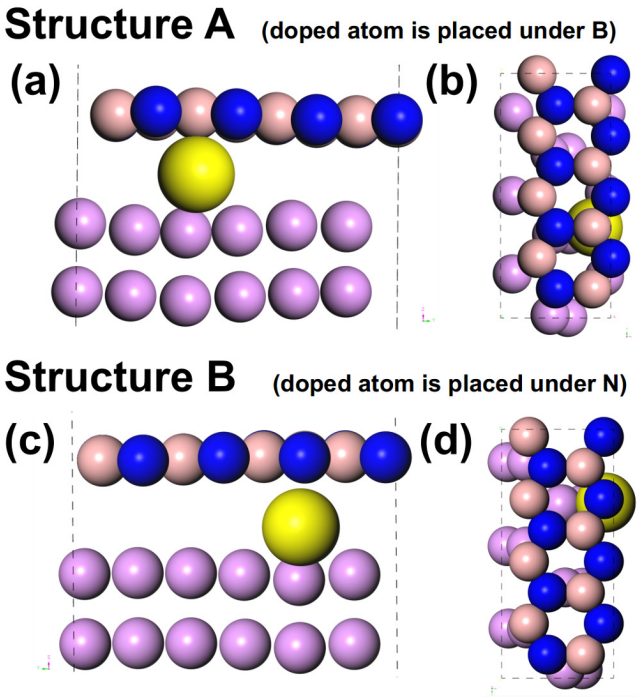

Fig. 1 Proposed configurations of single-atom-embedded h-BN/P heterostructure. Yellow, pink, blue, and purple sphere represent embedded atom(*M*), boron(B), nitrogen(N), and phosphorus, respectively: consequently, top and bottom layer indicates to be h-BN and P layer, respectively. Two embedded sites are designed: "Structure A" (See (a) and (b)) , and "Structure B" (See (c) and (d)). Note that *M* is consistent of (none), Na, Pd, Pt, Sc, Sn, Ti, Ag, Al, Au, and Fe.

The binding energy per atom(E_{bind}) is calculated to evaluated the stability of obtained ground state structure of pristine h-BN(BN)/P heterostructure and single-atom-embedded heterostructures. E_{bind} is calculated by the following equation 2.

$$E_{bind} = \frac{E_{P-BN} - (E_P + E_B + E_{doped})}{N_{atom}} \quad (2)$$

Where, E_{P-BN}, E_P, E_{BN},N_{atom} andE_{doped} represent total energy of h-BN(BN)/P heterostructures, total energy of P layer, total energy of BN layer, total number of constituent atom and total energy of doped atom(in bulk form) per an atom.

Additionally, the formation energy, the energy between two h-BN(BN) layers and single atom ($E_{formation}$), is calculated to consider the stability of the designed layer structure. $E_{formation}$ is calculated by the following equation 3.

$$E_{formation} = E_{total} - (E_P + E_{BN} + E_{doped}) \quad (3)$$

E_{total} represents the total energy of single atom embedded h-BN/P. Note that all negative energy represents the exothermic. The GLLB-sc functional[41] is used to obtain electronic structure and band gaps because pure DFT underestimates the band gap of semiconductors[42]. The GLLB-sc implemented calculations are carried out under the condition of k-point of (4,4,1) Brillouin zone sampling[33] with grid spacing of 0.18 Å. Note that the GLLB-sc implemented calculations are non-spin polarized due to the limitation of implementation on GPAW method. Projected density of states(PDOS) and Bader charge analysis[43–46] are obtained from calculation result from GLLB-sc functional in order to evaluate electronic properties.

Additionally, electronic band structures are obtained from GLLB-sc calculation to compare the electronic band alignment of h-BN/P.

Result and discussion

Ground states of all h-BN(BN)/P heterostructures are explored via first principles calculations. Effect of single-atom-embedded is evaluated by comparing between pristine h-BN/P and single-atom-embedded h-BN/P.

Pristine h-BN/P heterostructure

The designed pristine h-BN(BN)/P heterostructure reveals to be exothermic in both $E_{formation}$ and E_{bind}(-0.769 and -0.756 eV/atom, respectively), indicating to be energetically stable. The ground state h-BN/P heterostructure is scaled as 4.48 Åin x-axis and 9.97 Åin its unit cell. The interlayer distance is calculated to be 3.802 Å. The lattice mismatch is calculated as 2.51 % in x axis, and 0.33 % in y axis. The interlayer distance is estimated as 3.802 Åby the result of ground state optimization by vdW-DF functional. In particular, $E_{formation}$ is comparably stronger than the bond energy originate by van der Waals force. Electronic properties are evaluated by obtaining projector density of states(PDOS)(See Figure 4 (a)). PDOS of neighboring B(p-orbital), N(p-orbital), and P(p-orbital) is evaluated to consider the electronic interaction between layers. Note that PDOS is obtained by the calculation with GLLB-sc functional. PDOS reveals that orbitals of neighboring

B, N, and P atoms are remarkably overlapped in their orbitals in low energy level(See Figure 4 (a)). One can consider that strong $E_{formation}$ is originated from this overlap of orbitals, resulting to form strong covalent bond between layers. The band gaps of h-BN(BN)/P heterostructure is calculated with the GLLB-sc functional. h-BN(BN)/P heterostructure appeared to have similar direct band gap(2.425 eV) as well as that of single layer P(2.437 eV; See the band structure shown in Figure 2). To consider this band gap similarity, band structures of both h-BN(BN)/P heterostructure and single layer P are computed. The bandstructure of pristine h-BN/P has good agreement with previous work[47]. Both band structures indicate direct band gap in Γ valley band edge, with similar band alignment nearby Fermi level, which corresponds to the previous reports on h-BN/P heterostructure[47]. Thus, it can be concluded that pristine h-BN/P is similar to single layer P in terms of electronic property such as band gap.

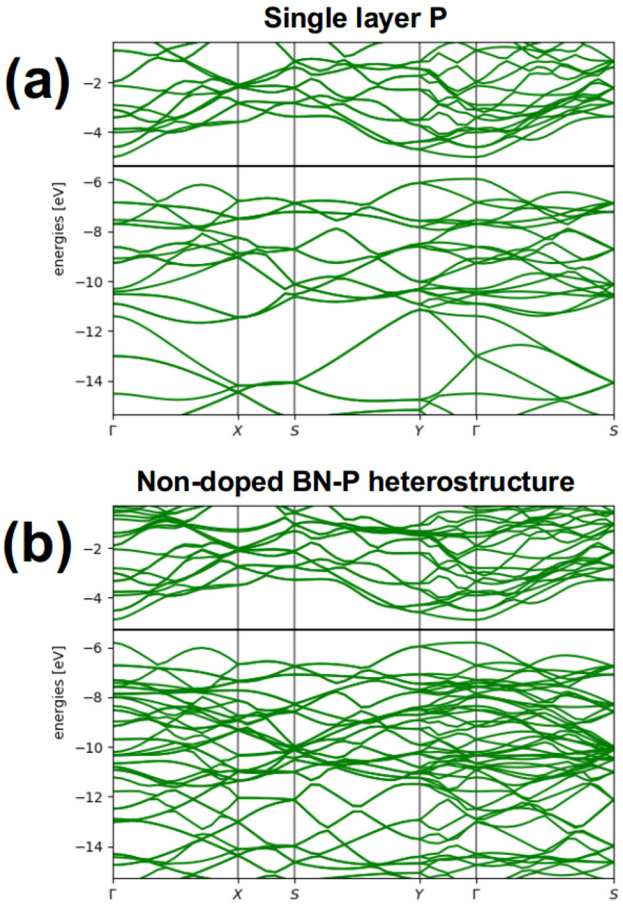

Fig. 2 The band structure of (a)Single layer P, and (b)Non-doped B-NP heterostructure.

Single-atom-embedded h-BN/P heterostructures

The ground state structures of single-atom-embedded h-BN/P are revealed via first principle calculations(See Table 1). It is notable that the distance from embedded atom(M) to the the neighboring P atom proportionally increases when single atom with larger single bond covalent radius(r_{cov}) is embedded in h-BN/P(See Table 1 and Figure 3). The lattice mismatch is calculated as 2.51% in x axis, and 0.33% in y axis.

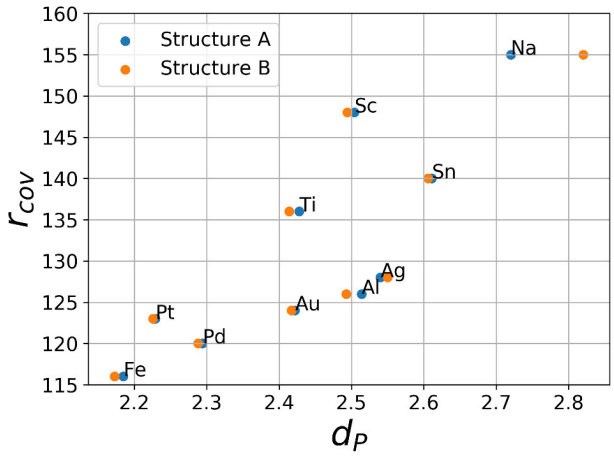

Fig. 3 The scatter plot of the distance from embedded atom(M) to the the neighboring P atom(unit: Å)(d_P) versus covalent radius(single bond) of embedded atom(r_{cov}). d_P reveals to increase as the existence of embedded-atom(M) with larger r_{cov}.

The calculated E_{bind} reveals to be exothermic with similar values(-0.732 $\sim$ -0.667) in all designed single-atom-embedded h-BN/P heterostructures, indicating that the stability of each BN and P layer are less effective in existence of embedding atom between layers. Meanwhile, $E_{formation}$ varies in each embedding atoms, indicating to affect the bonding state between h-BN and P layer. As a result, Na, Pd and Pt embedded heterostructure models are finally revealed to be exothermic both E_{bind} and $E_{formation}$(See Table 2) whereas Sc, Sn, Ti, Ag, Al, Au, and Fe doped heterostructures are exothermic in $E_{formation}$ in case of both “Structure A” and “Structure B” doped site(See 2). Projector density of states(PDOS) is obtained from the stable Na, Pd and Pt embedded heterostructures in order to consider the difference of their $E_{formation}$(See 2). Pt and Pd embedded heterostructures share similar trend in PDOS: embedded d-orbital of Pd and Pt sharply appears in the energy level from -1 to 5 eV in PDOS profiles in both "Structure A" and "Structure B"(See Figure 4 (c), (f), (d), and (g)). This indicates that Pt and Pd embedded heterostructures forms electron pairing among neighboring B, N and P atoms. Moreover, d-orbital of Pd and Pt is widely overlapped to the neighboring N(p-orbital) and P(p-orbital) orbitals in "Structure B" in the lower energy level(-5 $\sim$ eV) than those of "Structure A"(See Figure 1 (c), (f), (d), and (g)). One can consider that slightly higher $E_{formation}$ in "Structure B"(See Table 2) is originated from this wider orbital overlap in "Structure B".

On the other hand, Na embedded heterostructures shows different trend in PDOS(See Figure 4 (b) and (e)) to those of Pd and Pt embedded heterostructures. Remarkably, s-orbital of Na appears anti-bonding energy level(from 0 to 8 eV) in PDOS profiles and overlaps neighboring B(p-orbital) and P(p-orbital) orbitals in both "Structure A" and "Structure B"(See Figure 1); meanwhile Na embedded heterostructures have the most exothermic $E_{formation}$ in designed single atom embedded heterostuctures(See Table 2).

Table 1 Structure parameters of Single-atom-embedded h-BN/P heterostructures. d_B, d_N, d_P, $\angle_{BMP}$, and $\angle_{NMP}$ represent the distance from doped atom to the neighboring B atom(unit: Å), the distance from doped atom(M) to the neighboring N atom(unit: Å), the distance from embedded atom(M) to the the neighboring P atom(unit: Å), the angle among the neighboring B, doped atom(M), the neighboring P(unit: °), and the angle among the neighboring N, embedded atom(M), the neighboring P(unit: °), respectively.

Doped atom	**Structure A**(See Figure 1(a) and (b))			**Structure B**(See Figure 1(c) and (d))		
	d_B	d_P	$\angle_{BMP}$	d_N	d_P	$\angle_{NMP}$
Ag	2.766	2.540	138.5	2.742	2.550	134.4
Al	3.408	2.514	137.3	3.292	2.493	132.3
Au	2.944	2.422	138.2	2.812	2.417	136.4
Fe	2.582	2.185	109.8	2.316	2.173	126.0
Na	2.520	2.720	137.8	2.780	2.820	123.2
Pd	2.889	2.294	122.4	2.580	2.288	130.3
Pt	2.851	2.229	115.3	2.504	2.226	134.6
Sc	2.468	2.504	130.6	2.676	2.494	103.1
Sn	3.565	2.611	141.2	3.608	2.606	137.5
Ti	2.484	2.428	110.7	2.494	2.414	113.2

Charge transfer is evaluated by Bader charge analysis[43–46] by using the calculated result with GLLB-sc functional, in order to evaluate how charge is transferred among doped atom and neighboring atoms. The result of Bader charge analysis is available on the supporting information.

Na-embedded heterostructures are positively charged in embedded Na atom in both "Structure A" and "Structure B"(positively charged 0.860 and 0.958 electrons, respectively). Subsequently, the neighboring P is negatively charged 0.339 and 0.181 electrons respectively, indicating the electronic charge is transferred from embedded Na to the neighboring P. On the contrary, Pd and Pt embedded heterostructures are all negatively charged in embedded Pd(Pt) atom in both "Structure A" and "Structure B"(See Table 3). In comparison with previous studies, it is reported that Na holds 0.779 electron in Na embedded h-BN/P heterostructure with 0 ÎijB for the spin magnetic moment[31]. This shows good agreement with those of this work as shown in Tables 2 and 3.[31])

The band gap is calculated with the GLLB-sc functional in terms of accurate estimation of band gap to the experimental value[42]. Na, Pd, and Pt atom-embedded h-BN(BN)/P heterostructures reveal to have narrower band gap than pristine h-BN(BN)/P heterostructure(=2.425 eV)(See Table 4). Remarkably, band gaps of atom-embedded heterostructures (1.5∼1.8 eV) are suitable for solar energy conversion[48]. One can consider that the designed atom-embedded heterostructures are promising materials for solar energy driven electronic device with band gap tunability by changing embedded atom. This band gap transition is considered to originate from the energy shit of p-orbital in P near to the embedded atom(See the PDOS shown in Figure 4); the p-orbital in P is commonly located around the Fermi level in all h-BN(BN)/P heterostructures. The band structures are additionally computed to evaluate how electronic structures are shifted by the single atom embedding. Commonly, both pure- and atom-embedded h-BN(BN)/P heterostructures share their direct band gap at Γ point in band structures(See Figure 2 and Figure 5). Thus, the direct band gap reduces its value by single-atom-embedding because of the transition of p-orbital of P.

Electronic structures are computed in Na, Pd and Pt embedded h-BN(BN)/P heterostructures with GLLB-sc functional as well

Table 2 The physical parameters evaluated by the result obtained by calculations with vdW-DF functional. $E_{formation}$, E_{bind}, and m_{doped} represent the interlayer binding energy of BN-P heterostructure(unit: eV), binding energy of BN-P heterostructure per atom(unit: eV/atom), and magnetic moment of doped atom(unit:μ_B) respectively. Note that negative energy is exothermic.

Doped atom	$E_{formation}$	E_{bind}	m_{doped}
(None)	-0.769	-0.756	n.a
Structure A(See Figure 1(a) and (b))			
Ag	0.595	-0.683	0.00
Al	0.651	-0.681	0.00
Au	0.583	-0.683	0.00
Fe	0.699	-0.679	1.99
Na	**-0.812**	-0.731	0.00
Pd	**-0.383**	-0.716	0.00
Pt	**-0.009**	-0.704	0.00
Sc	0.089	-0.700	0.00
Sn	1.049	-0.667	0.00
Ti	0.634	-0.681	1.84
Structure B(See Figure 1(c) and (d))			
Ag	0.583	-0.683	0.00
Al	0.692	-0.679	0.00
Au	0.577	-0.683	0.00
Fe	0.655	-0.681	1.99
Na	**-0.829**	-0.732	0.00
Pd	**-0.484**	-0.720	0.00
Pt	**-0.005**	-0.703	0.00
Sc	0.057	-0.701	0.00
Sn	1.050	-0.667	0.00
Ti	0.494	-0.686	1.88

Table 3 The charge transfer evaluated within Bader charge analysis[43–46] result by using calculated result with GLLB-sc functional. Q_{doped}, $Q_{B_{near}}$, $Q_{N_{near}}$, and $Q_{P_{near}}$ represent charge transfer of doped atom, charge transfer of neighboring B to the doped atom, charge transfer of neighboring N to the doped atom, and charge transfer of neighboring P to the doped atom, respectively.As a reference, whole bader charge analysis result is provided in the supporting information.

Doped atom	Q_{doped}	$Q_{B_{near}}$	$Q_{N_{near}}$	$Q_{P_{near}}$
Structure A(See Figure 1(a) and (b))				
Na	0.860	2.282	-	-0.339
Pd	-0.716	2.259	-	-0.039
Pt	-1.877	2.250	-	-0.007
Structure B(See Figure 1(c) and (d))				
Na	0.958	-	-2.230	-0.181
Pd	-0.982	-	-2.393	-0.112
Pt	-1.523	-	-2.345	0.049

Table 4 The calculated result of GLLB-sc functional in stable state of stable BN-P heterostructures. E_g, $E_{g(KS)}$, and Deriv. represents fundamental band gap, Kohn-Sham band gap and derivative discontinuity[41], respectively.

Doped atom	$E_{g(KS)}$	Deriv.	E_g
(None)	1.664	0.761	2.425
Structure A(See Figure 1(a) and (b))			
Na	1.112	0.506	1.618
Pd	1.203	0.548	1.751
Pt	1.089	0.487	1.576
Structure B(See Figure 2(c) and (d))			
Na	1.116	0.507	1.623
Pd	1.217	0.547	1.764
Pt	1.031	0.465	1.496

as non-embedded h-BN(BN)/P heterostructures and single layer P(See Figure 2 and Figure 3). The calculated band structures reveal to have the direct band gap in Γ point(See Figure 2 and Figure 5) in all designed Na, Pd, and Pt embedded h-BN(BN)/P heterostructures.

Conclusions

Pristine- and single-atom-embedded- h-BN(BN)/P bilayer heterostructures are investigated via first principles calculations. In particular, the thermodynamic stability is evaluated in the pristine-, Na-, Pd-, Pt-, Sc-, Sn-, Ti-, Ag-, Al-, Au-, and Fe- embedded heterostructures. The pristine h-BN(BN)/P heterostructures are thermodynamically stable as well as single layer P and h-BN. On the other hand, the thermodynamic stability of single-atom-embedded- h-BN(BN)/P heterostructures revealed to be dependent on the embedded atom kind; Na, Pd and Pt are exothermic while rest of Sc, Sn, Ti, Ag, Al, Au, and Fe turn out to be endothermic. Thus, the stable Na, Pd and Pt -embedded- h-BN(BN)/P heterostructures are focused to evaluate the transition of physical properties. Remarkably, the single-atom-embedded heterostructure reveals to have narrower direct band gaps(1.5∼1.8 eV) than pristine h-BN(BN)/P heterostructures(=2.425 eV) by the calculation with GLLB-sc functional band gap correction. The narrower band gaps are on the suitable range for optoelectronic application such as solar energy driven electronic device materials. Thus, one can consider that the single-atom-embedded h-BN(BN)/P heterostructures are potential for optoelectronic materials with the availability in band gap tuning by controlling its embedding atom.

Conflicts of interest

The authors declare no competing financial interests.

Acknowledgements

This study was partly funded by Japan Science and Technology Agency (JST) CREST Grant Number JPMJCR17P2, and JSPS KAKENHI Grant-âĂŘinâĂŘ-Aid for Young Scientists (B) Grant Number JP17K14803.

Notes and references

1 K. S. Novoselov, D. Jiang, F. Schedin, T. Booth, V. Khotkevich, S. Morozov and A. K. Geim, *Proceedings of the National Academy of Sciences*, 2005, **102**, 10451–10453.

2 A. K. Geim and K. S. Novoselov, *Nanoscience and Technology: A Collection of Reviews from Nature Journals*, World Scientific, 2010, pp. 11–19.

3 M. E. Dávila, L. Xian, S. Cahangirov, A. Rubio and G. L. Lay, *New Journal of Physics*, 2014, **16**, 095002.

4 L. Li, S.-z. Lu, J. Pan, Z. Qin, Y.-q. Wang, Y. Wang, G.-y. Cao, S. Du and H.-J. Gao, *Advanced Materials*, 2014, **26**, 4820–4824.

5 L. Li, Y. Yu, G. J. Ye, Q. Ge, X. Ou, H. Wu, D. Feng, X. H. Chen and Y. Zhang, *Nature nanotechnology*, 2014, **9**, 372.

6 H. Liu, A. T. Neal, Z. Zhu, Z. Luo, X. Xu, D. Tománek and P. D. Ye, *ACS nano*, 2014, **8**, 4033–4041.

7 S. P. Koenig, R. A. Doganov, H. Schmidt, A. H. Castro Neto and B. Özyilmaz, *Applied Physics Letters*, 2014, **104**, 103106.

8 A. Carvalho, M. Wang, X. Zhu, A. S. Rodin, H. Su and A. H. C. Neto, *Nature Reviews Materials*, 2016, **1**, 16061.

9 A. Ziletti, A. Carvalho, D. K. Campbell, D. F. Coker and A. H. Castro Neto, *Phys. Rev. Lett.*, 2015, **114**, 046801.

10 F. Iyikanat, E. Torun, R. T. Senger and H. Sahin, *Phys. Rev. B*, 2019, **100**, 125423.

11 F.-f. Zhu, W.-j. Chen, Y. Xu, C.-l. Gao, D.-d. Guan, C.-h. Liu, D. Qian, S.-C. Zhang and J.-f. Jia, *Nature materials*, 2015, **14**, 1020–1025.

12 L. Takahashi and K. Takahashi, *Physical Chemistry Chemical Physics*, 2015, **17**, 21394–21396.

13 D. Di Sante, P. Eck, M. Bauernfeind, M. Will, R. Thomale, J. Schäfer, R. Claessen and G. Sangiovanni, *Phys. Rev. B*, 2019, **99**, 035145.

14 K. Kobayashi and J. Yamauchi, *Phys. Rev. B*, 1995, **51**, 17085–17095.

15 C. Sevik, *Phys. Rev. B*, 2014, **89**, 035422.

16 T. Habe and M. Koshino, *Phys. Rev. B*, 2017, **96**, 085411.

17 X.-X. Zhang, Y. Lai, E. Dohner, S. Moon, T. Taniguchi, K. Watanabe, D. Smirnov and T. F. Heinz, *Phys. Rev. Lett.*, 2019, **122**, 127401.

18 D. Akinwande, N. Petrone and J. Hone, *Nature communications*, 2014, **5**, 1–12.

19 W. Zhou, S. Zhang, S. Guo, Y. Wang, J. Lu, X. Ming, Z. Li, H. Qu and H. Zeng, *Phys. Rev. Applied*, 2020, **13**, 044066.

20 A. K. Geim and I. V. Grigorieva, *Nature*, 2013, **499**, 419–425.

21 K. Novoselov, A. Mishchenko, A. Carvalho and A. C. Neto, *Science*, 2016, **353**, aac9439.

22 Y. Liu, N. O. Weiss, X. Duan, H.-C. Cheng, Y. Huang and X. Duan, *Nature Reviews Materials*, 2016, **1**, 1–17.

23 Z. Liu, L. Song, S. Zhao, J. Huang, L. Ma, J. Zhang, J. Lou and P. M. Ajayan, *Nano letters*, 2011, **11**, 2032–2037.

24 S. Zhang, Z. Yan, Y. Li, Z. Chen and H. Zeng, *Angewandte Chemie International Edition*, 2015, **54**, 3112–3115.

25 Y. Gong, S. Lei, G. Ye, B. Li, Y. He, K. Keyshar, X. Zhang, Q. Wang, J. Lou, Z. Liu *et al.*, *Nano letters*, 2015, **15**, 6135–6141.

26 B. Zhai, J. Du, C. Shen, T. Wang, Y. Peng, Q. Zhang and C. Xia, *Phys. Rev. B*, 2019, **100**, 195307.

27 M. Si, P.-Y. Liao, G. Qiu, Y. Duan and P. D. Ye, *Acs Nano*, 2018, **12**, 6700–6705.

28 W. Zhou, X. Liu, X. Hu, S. Zhang, C. Zhi, B. Cai, S. Guo, X. Song, Z. Li and H. Zeng, *Nanoscale*, 2018, **10**, 15918–15925.

29 W. Zhang and W. Zheng, *Advanced Functional Materials*, 2016, **26**, 2988–2993.

30 K. Takahashi and L. Takahashi, *ACS Applied Electronic Materials*, 2018, **1**, 2–6.

31 C. Wang, J. Sun, B. Zhang, J. Zhang and X. Tao, *Applied Surface Science*, 2017, **423**, 1003–1011.

32 J. J. Mortensen, L. B. Hansen and K. W. Jacobsen, *Phys. Rev. B*, 2005, **71**, 035109.

33 H. J. Monkhorst and J. D. Pack, *Physical review B*, 1976, **13**, 5188.

34 M. Dion, H. Rydberg, E. Schröder, D. C. Langreth and B. I. Lundqvist, *Phys. Rev. Lett.*, 2004, **92**, 246401.

35 A. Priydarshi, Y. S. Chauhan, S. Bhowmick and A. Agarwal, *Phys. Rev. B*, 2018, **97**, 115434.

36 G. Gao, Y. Jiao, E. R. Waclawik and A. Du, *Journal of the American Chemical Society*, 2016, **138**, 6292–6297.

37 T. Tong, B. Zhu, C. Jiang, B. Cheng and J. Yu, *Applied Surface Science*, 2018, **433**, 1175–1183.

38 Z. Lu, P. Lv, Z. Yang, S. Li, D. Ma and R. Wu, *Physical Chemistry Chemical Physics*, 2017, **19**, 16795–16805.

39 S.-L. Li, H. Yin, X. Kan, L.-Y. Gan, U. Schwingenschlögl and Y. Zhao, *Physical Chemistry Chemical Physics*, 2017, **19**, 30069–30077.

40 Z. Wei, Y. Zhang, S. Wang, C. Wang and J. Ma, *Journal of Materials Chemistry A*, 2018, **6**, 13790–13796.

41 M. Kuisma, J. Ojanen, J. Enkovaara and T. T. Rantala, *Phys. Rev. B*, 2010, **82**, 115106.

42 F. Tran, S. Ehsan and P. Blaha, *Phys. Rev. Materials*, 2018, **2**, 023802.

43 M. Yu and D. R. Trinkle, *The Journal of Chemical Physics*, 2011, **134**, 064111.

44 G. Henkelman, A. Arnaldsson and H. Jónsson, *Computational Materials Science*, 2006, **36**, 354–360.

45 E. Sanville, S. D. Kenny, R. Smith and G. Henkelman, *Journal of Computational Chemistry*, 2007, **28**, 899–908.

46 W. Tang, E. Sanville and G. Henkelman, *Journal of Physics: Condensed Matter*, 2009, **21**, 084204.

47 Y. Cai, G. Zhang and Y.-W. Zhang, *The Journal of Physical Chemistry C*, 2015, **119**, 13929–13936.

48 M. M. Lee, J. Teuscher, T. Miyasaka, T. N. Murakami and H. J. Snaith, *Science*, 2012, **338**, 643–647.

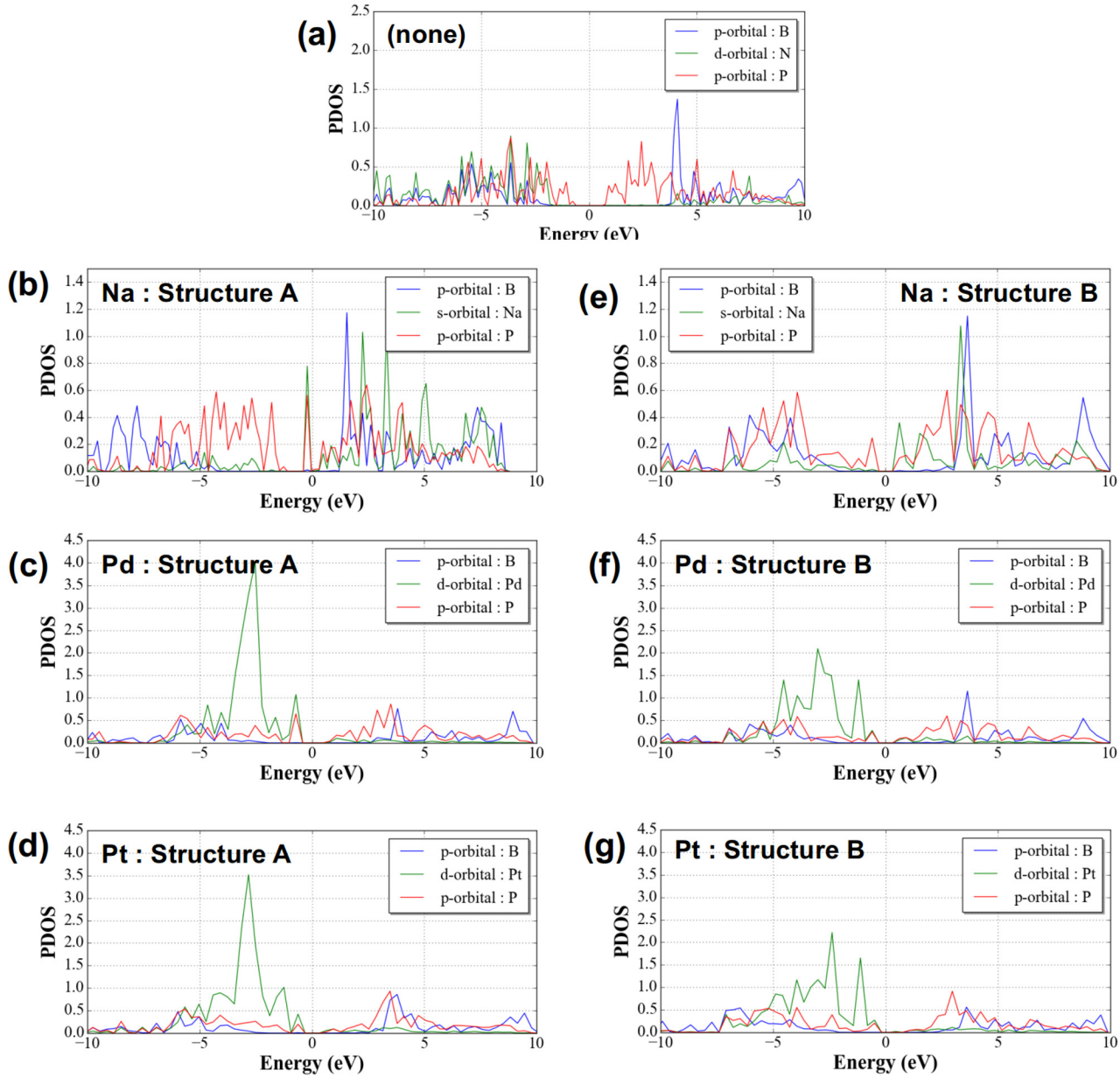

Fig. 4 The projected density of states(PDOS) calculated by GLLB-sc functional. Each picture represents the PDOS of (a)Na doped heterostructure, (b)Pd doped heterostructure, (c)Pt doped heterostructure of "Structure A", and (d)Na doped heterostructure, (e)Pd doped heterostructure, (f)Pt doped heterostructure of "Structure B", respectively. Note that showing B, P and N atom are neighboring to doped atom.

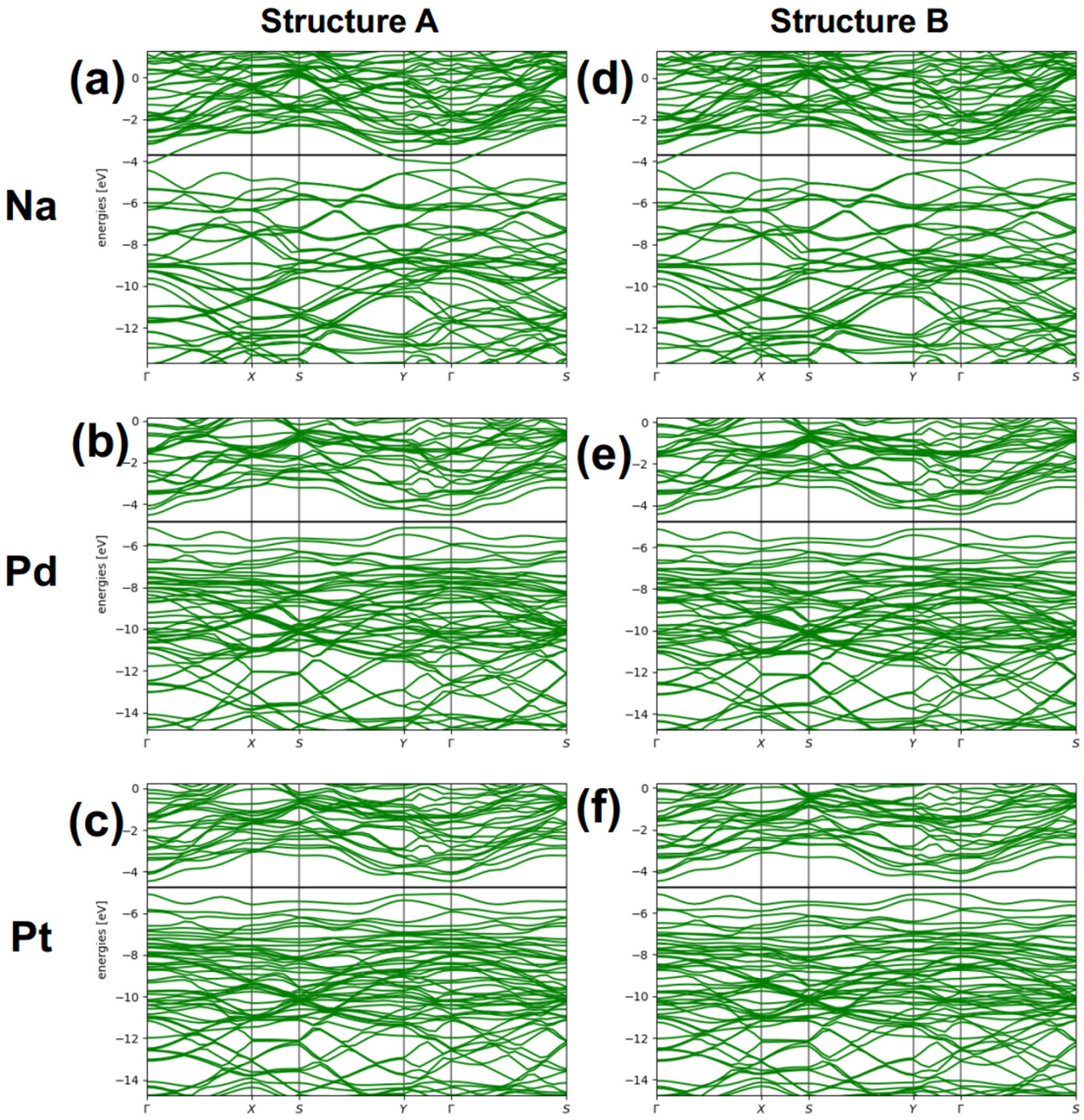

Fig. 5 The band structure of Na, Pd and Pt doped BN-P heterostructures with GLLB-sc functional.(a)Na doped heterostructure(Structure A), (b)Pd doped heterostructure(Structure A), (c)Pt doped heterostructure(Structure A), (d)Na doped heterostructure(Structure B), (e)Pd doped heterostructure(Structure B), and (f)Pt doped heterostructure(Structure B)